


Crack incubation in shot peened AA7050 and mechanism for fatigue enhancement

Daniel J. Chadwick¹ | Siavash Ghanbari² | David F. Bahr² | Michael D. Sangid^{1,2} 

¹ School of Aeronautics and Astronautics, Purdue University, 701 W. Stadium Ave, West Lafayette, IN 47907-2045, USA

² School of Materials Engineering, Purdue University, 701 W. Stadium Ave, West Lafayette, IN 47907-2045, USA

Correspondence

Michael D. Sangid, School of Aeronautics and Astronautics, Purdue University, 701 W. Stadium Ave, West Lafayette, IN 47907-2045, USA.

Email: msangid@purdue.edu

Funding information

Royal Australian Air Force; Purdue's Center for Surface Engineering and Enhancement; Office of Naval Research, Grant/Award Number: N00014-14-1-0544

Abstract

Shot peening is a dynamic cold-working process involving the impingement of peening media onto a substrate surface. Shot peening is commonly used as a surface treatment technique within the aerospace industry during manufacturing to improve fatigue performance of structural components. The compressive residual stress induced during shot peening results in fatigue crack growth retardation, improving the performance of shot-peened components. However, shot peening is a compromise between the benefit of inducing a compressive residual stress and causing detrimental surface damage. Because of the relatively soft nature of AA7050-T7451, shot peening can result in cracking of the constituent precipitate particles, creating an initial damage state. The aim of this paper is to understand the balance and fundamentals of these competing phenomena through a comparative study throughout the fatigue lifecycle of baseline versus shot-peened AA7050-T7451. Microstructure and surface topology characterization and comparison of the baseline and shot-peened AA7050-T7451 has been performed using scanning electron microscopy, electron backscatter diffraction, energy dispersive spectroscopy, and optical profilometry techniques. A residual stress analysis through interrupted fatigue of the baseline and shot-peened AA7050-T7451 was completed using a combination of X-ray diffraction and nanoindentation. The fatigue life performance of the baseline versus shot-peened material has been evaluated, including crack initiation and propagation. Subsurface particles crack upon shot peening but did not incubate into the matrix during fatigue loading, presumably due to the compressive residual stress field. In the baseline samples, the particles were initially intact, but upon fatigue loading, crack nucleation was observed in the particles, and these cracks incubated into the matrix. In damage tolerant analysis, an initial defect size is needed for lifetime assessment, which is often difficult to determine, leading to

Nomenclature: (*hkl*), Miller indices; 2θ , Diffraction angle; A_c , A , A_o , Corrected contact area, contact area for the residual stress measurement, and contact area in stress free sample, respectively; C , Measure of curvature on loading ramp of load/depth curve (compliance); d , d_o , d_ψ , Lattice spacing (reference value and sample at orientation ψ); E , Elastic (Young's) modulus; E_r , Reduced elastic modulus; H , Hardness; h , Indent Depth; N , Number of fatigue cycles; n , Positive integer; P , P_{max} , Indent force (maximum); R , Stress ratio; S , Stiffness at initial unloading; α , Angle between indenter and contact surface; β , Indent geometry constant (Berkovich); λ , wavelength; ν , Poisson's ratio; σ_{max} , Maximum stress during fatigue loading; σ_{min} , Minimum stress during fatigue loading; σ_{SG} , Residual stress from nanoindentation via Suresh and Giannakopoulos model; σ_{XRD} , Biaxial residual stress from X-ray diffraction; ψ , Orientation of sample angle

Abbreviations: EBSD, Electron backscatter diffraction; L-T, Longitudinal-transverse; SEM, Scanning electron microscope; XRD, X-ray diffraction

overly conservative evaluations. This work provides a critical assessment of the mechanism for shot peening enhancement for fatigue performance and quantifies how incubation of a short crack is inhibited from an initially cracked particle into the matrix within a residual stress field.

KEYWORDS

AA7050, crack incubation, fatigue, nanoindentation, particle cracking, residual stresses, shot peening

1 | INTRODUCTION

For many years, shot peening has been widely used for fatigue enhancement of aluminum alloy components within the aerospace industry. Shot peening consists of numerous elasto-plastic impacts of media onto the surface of a workpiece, which contributes to the formation of a residual stress field. The goal is to produce a compressive residual stress field that is uniform across the surface and also extends into the subsurface of the workpiece. The shot peening process is a compromise between a beneficial residual stress field produced and surface and near-subsurface damage. With the trend of lightweighting in the aerospace community, more airframe components contain thin webs, which requires a need to understand and quantify this engineering trade-off in thinned-walled structures.

It is widely accepted that the fatigue enhancement due to shot peening is attributed to the compressive residual stress field.¹⁻⁷ Crack growth rates were approximately 2 to 4 times slower for shot-peened samples versus baseline samples for short cracks, but the growth rates were approximately the same for longer cracks.⁶ Shot peening a material containing small cracks has been shown to restore the material's endurance limit to within approximately 10% of its original value.⁶ Further, the relaxation of residual stress profile is of critical importance, since severe relaxation can cause a degradation of the material's fatigue performance.^{2,3,8,9} Stress relaxation can be attributed to mechanical or thermal loading resulting in plastic deformation.

Shot peening has proven to be ineffective in increasing fatigue life in cases of poor surface finish.⁷ Hence, the surface damage from shot peening plays a significant role in determining the life. Following shot peening, a material's surface can be smoothed to further increase the life by approximately 10%,⁷ such techniques include electropolishing,¹⁰ fine particle shot peening,^{11,12} double shot peening (with a finer shot media),^{13,14} and secondary surface treatments (superfinishing,¹⁵ vibrostrengthening,¹⁶ etc). Since material is removed during the majority of these processes, it is paramount that sufficient subsurface residual stresses are developed during the initial shot peening process to enhance the fatigue life. Several models exist for the competing

mechanisms to predict fatigue behavior influenced by surface roughness and residual stresses.^{2,17,18} Additional process modeling efforts also predict the residual stress fields and surface roughness resulting from the shot peening process.¹⁹⁻²¹

Sharp and Clark note that for aerospace aluminum the crack initiation period is shorter after shot peening due to surface damage, although the total fatigue life is enhanced.⁷ Of particular interest in this paper is AA7050, a common airframe material. Through a detailed study of (unpeened) AA7050 material, Barter et al concluded that secondary constituent particles, specifically $\text{Al}_7\text{Cu}_2\text{Fe}$, Mg_2Si , and Al_2CuMg , were the primary sites for crack initiation.²² After analyzing approximately a thousand cracks, they observed crack initiation occurs predominantly in particles greater than 6 μm located immediately subsurface.²² Ingraffea and coworkers observed the fracture of $\text{Al}_7\text{Cu}_2\text{Fe}$ constituent particles is the major crack incubation source in unpeened AA7075. Through modeling they developed a response surface to predict the tensile stress in the particle as a function of the strain in the adjacent matrix, surrounding grain orientations, and aspect ratio²³ and further the formation of microstructurally short crack formation in the matrix material.^{24,25} In shot-peened steel, McDowell and coworkers modeled the compromise between inclusion cracking and residual stress in the matrix, concluding that a partially bonded inclusion resulted in the lowest fatigue life.^{26,27} Since particle cracking is known to be critical in fatigue life of Al alloys, a detailed analysis is necessary of the mechanisms behind shot peening, especially subsurface, where cracks are more likely to initiate.

The paper addresses the question of what is the mechanism of shot-peening enhancement for fatigue performance in airframe, high strength Al alloys by quantifying how a cracked particle starts to incubate the short crack into the matrix within a residual stress field, at what stage of the fatigue life this occurs, and if shot peening has an effect upon the phenomenon, as summarized in Figure 1. It is well accepted in the literature that shot peening provides a fatigue enhancement for AA7050, the material of interest within this study. A statistical analysis for the comparisons of fatigue lives between the baseline and shot-peened cases in AA7050 is beyond the scope of the current work; and for such data, the reader is referred to many such works on this

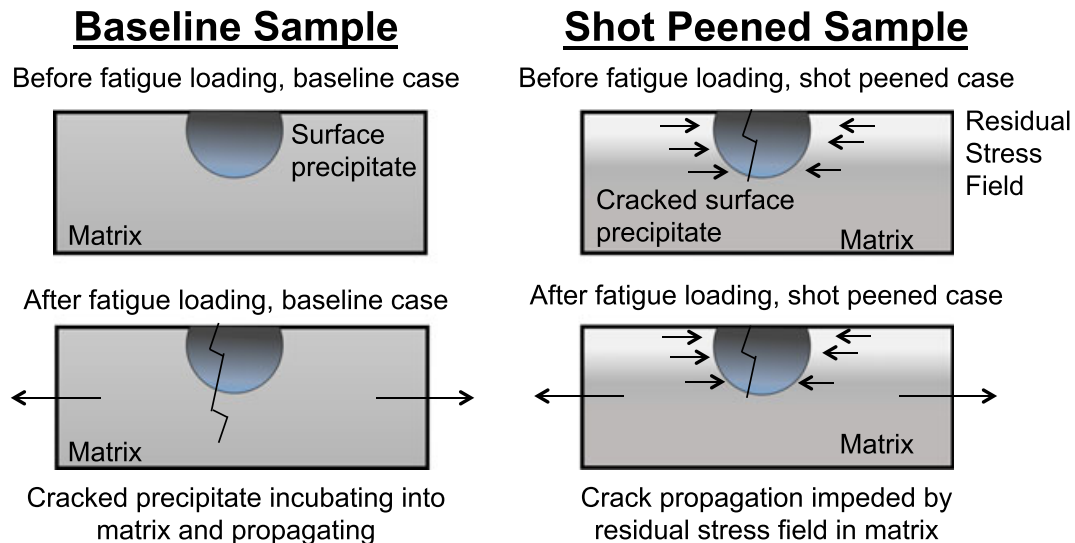


FIGURE 1 Comparison of theorized precipitate cracking state, baseline and shot peened samples, and before and after fatigue loading [Colour figure can be viewed at wileyonlinelibrary.com]

subject, Luong and Hill,²⁸ Carvalho and Voorwald,^{29,30} Gao,³¹ and Bae³² to name a few. The paper is outlined as follows. The experimental methodology, including material, specimen, shot peening, and fatigue loading parameters, and characterization details are described in Section 2. The effects of shot peening, specifically surface roughness, sub-surface residual stresses, and microstructure are quantified in Section 3. Section 4 reviews the particle cracking of the $\text{Al}_7\text{Cu}_2\text{Fe}$ particles and their evolution during fatigue loading via electron microscopy imaging and nanoindentation measurements. The role of the residual stress in the Al matrix is described in Section 5, including X-ray diffraction (XRD) quantification and nanoindentation.

2 | EXPERIMENTAL METHODOLOGY

2.1 | Material and specimen design

The material used in this study is an aerospace grade aluminum alloy, AA7050. The material is tempered in the T7451 condition and produced in plate form, according to specification³³ AMS 4050. From the rolled plate material AA7050-T7451, a set of flat dog bone samples were machined in the longitudinal-transverse (L-T) direction, at least 6.4 mm from the outside surface of the plate to avoid any edge effects of the rolling process. The samples have a nominal thickness of 1.6 mm and a gauge section, 3 mm in width and 10 mm in length. A $10 \times 10 \times 1.6$ mm section at each end gives the distinctive dog bone appearance, with this grip section used during fatigue loading for load transfer. The samples have an overall length of 48 mm. The specimen geometry was adapted from the ASTM E8 standard,³⁴ such that the

dimensions were compatible for characterization within a scanning electron microscope (SEM). Moreover, as previously mentioned, the thin specimens are representative of the industrially relevant application for shot peening of thin-walled aerospace components. For full-mechanical characterization of the samples in the L-T direction, please refer to Mello et al.³⁵

2.2 | Shot peen processing

All samples were roughly polished using a fixed speed Buehler Ecomet V Grinder-Polisher, and a 1200-grit sand paper for 2 minutes under lubrication with water. The samples in the as machined and polished condition will be referred to as the baseline case throughout the remainder of the paper. At this point, 5 samples were shot peened commercially.* Samples were shot peened on all faces, in a staged peening process involving fixing the samples onto a flat backing whilst the opposite side was peened. The peening media used for shot was a Z150 ceramic zirconia, with constituents including ~68% zirconia (ZrO_2) and ~32% vitreous phase (SiO_2 and Al_2O_3). The shot particle size ranges from 100 to 210 μm diameter. The shot was pressure blasted through a 7.94-mm V-type nozzle at a pressure of 41.4 kPa, with a 45° angle of impingement from the horizontal surface, and a 152.4 mm standoff distance. To quantify the peening parameters, saturation tests were performed on 2 Almen intensity, type N, test strips prior to the process. Exposure was measured as number of passes over the test strip, and

*Peening was performed by Progressive Surface (Grand Rapids, Michigan), in consultation with Electronics, Inc (Mishawaka, Indiana) regarding specific peening conditions suitable for thin gauge aluminum.

the resultant arc height was recorded. Based on this analysis, a total of 23 passes were conducted on all sides of the specimen to ensure complete coverage of the shot peening, which corresponds to an Almen intensity value of 6. Following this process, samples were visually inspected for any warping or out of plane deformation, symptoms of a significant imbalance of residual stress. All samples remained free of warping and splitting following the peening process. Throughout this paper, these 5 samples shall be referred to as the shot-peened subset.

2.3 | Specimen preparation

All samples were polished (1200-grit sand paper disc for 2 minutes under lubrication with water) to remove machining marks. However, this surface treatment still exhibited scratches and nonuniformity of the sample surface. Finer polishing techniques were required to successfully obtain the surface uniformity that is compatible with electron backscatter diffraction (EBSD) analysis techniques.

For the shot-peened samples, an incremental polishing process was conducted. The intention of this process was to evaluate the depth of surface roughness that would need to be removed to conduct electron microscopy on a uniform surface. Polishing was carried out using the Ecomet V Grinder-Polisher, and a series of short 2-minute exposures to a Pace Technologies NAPPAD 8" polishing pad lubricated with distilled water and a 0.05 μm colloidal silica suspension. At each stage, an optical image was obtained using an Olympus BX51M optical microscope to visually inspect the surface condition. The sample thickness was measured before and after the polishing process, with a Mitutoyo IP-65 Micrometer. Approximately 90 μm of material was required to be removed to exposure a uniform and planar surface. Once a uniform surface was achieved, microscratches, which were still evident, needed to be removed prior to any electron microscopy for both the baseline and shot-peened cases. A polishing process, consisting of a simple 1200-grit sand paper for 2 minutes with distilled water lubrication, followed by a 40-min fine polish using the 0.05- μm colloidal silica and an excess of distilled water, was performed to achieve a uniform, flat, and mirror-like surface. On each sample, the surface of interest for the subsequent microstructure characterization and micromechanical testing was polished to a mirrored-like sample, while the opposite face was left in the as shot-peened condition.

To secure a consistent point of reference upon the samples, fiducial markers were employed. Following polishing, a Vickers Leco micro hardness tester LM247AT was used to place indents marking areas of interest (1000 μm \times 1000 μm in size). The indents were formed using a loading at 200 g of indentation force and effectively labeled.

2.4 | Fatigue loading parameters

A servo-hydraulic drive MTS load frame was used for the fatigue loading. The MTS load cell consists of a model 244.12 hydraulic ram (actuator), capable of loading up to 25 kN, in combination with an MTS 661.20E-01 load cell (transducer), capable of sensing loads of up to 25 kN. The gripping mechanisms used were MTS 647 hydraulic wedge grips, capable of gripping pressure up to 21 MPa. The maximum stress was chosen as $\sim 85\%$ of the material's tensile yield strength, 469 MPa as measured from.³⁵ Thus, the load range was 20 to 400 MPa, resulting in a stress ratio of 0.05 to avoid any potential buckling of the specimen. This ensured that the fatigue loading regime remained within the elastic region of the material. For the MTS load frame, the cyclic frequency was also analyzed through a force command versus force measured comparison for a range of frequencies (0.67 to 9 Hz). A frequency of 3 Hz was chosen as a compromise between efficient cyclic loading and to minimize control errors. The fatigue testing parameters are given in Table 1.

A sequence of which would enable the iterative analysis at varied levels of fatigue cycling ($N = 0, 1, 10, 100, 1000, 10\ 000, \text{ and } 15\ 000$) was used. Strain measurements were taken with a MTS model 632.26 B30 extensometer. The hysteresis (stress-strain) data ensured the loading remained in the elastic regime throughout the life cycle for both the baseline and shot-peened samples.

2.5 | Material characterization

The EBSD was performed in a FEI Philips XL-40 SEM. The area of interest was identified upon the sample surface, and an EBSD scan was conducted with a 4 μm step size. The cleanup process involved removal of data points with confidence interval less than 0.05, and filtering and removal of disparate, isolated, and very small orientations utilizing the OIM Analysis Software Version 6.1 postprocessing functions. The presence of the secondary phase (precipitates) is not accounted for during the EBSD process, as the material is considered to be pure homogenous aluminum for analysis. To identify precipitates energy dispersive X-ray spectroscopy was used to conduct elemental analysis. Surface roughness characterization (topography) was performed using a Zegage

TABLE 1 Fatigue testing parameters

Parameter	Value
Maximum stress, σ_{max}	400 MPa
Minimum stress, σ_{min}	20 MPa
Frequency	3 Hz
Stress ratio, R	0.05
Loading shape	Sinusoidal
Gripping mechanics	10 MPa in hydraulic wedge

3D Optical Profiler. This is a noncontact, light interferometry device, which was used for quantitative measurements of sample surface profiles.

X-ray diffraction was performed in PanAnalytical X'Pert 2 XRD system. The system comprised of a Cu point focus X-ray source, primary optics of X-ray lens, secondary optics of anti-scatter slits, a radiation wavelength of 0.15418 nm (Cu K alpha 1 and K alpha 2), and a PIXcel point detector. For each sample, a peak scan was conducted, to generate a diffraction peak profile. The $\sin^2\psi$ technique was used for residual stress calculation. This technique involves the linear regression trend line fitting to multiple psi (ψ) angle measurements, from which a stressed lattice spacing average is derived, d , and then subsequently the biaxial residual stress value σ_{XRD} was found by

$$\sigma_{\text{XRD}} = \left(\frac{E}{1 + \nu} \right)_{(hkl)} \frac{1}{d_0} \left(\frac{\delta d_\psi}{\delta \sin^2 \psi} \right). \quad (1)$$

With E and ν , being Elastic modulus and Poisson ratio, (hkl) being Miller indices, and d_0 and d_ψ representing lattice spacing at a reference and about the ψ orientation. For all scans, the $[4, 0, 0]$ Miller index peak was utilized for residual stress determination.

The nanoindentation procedure was undertaken using a Hysitron TI950 TribIndenter, in conjunction with a Berkovich pyramid indentation tip. During indentation the applied force, P , and the indentation depth, h , are recorded. The Oliver-Pharr method was used to determine the hardness, H , and reduced modulus, E_r ,^{36,37}:

$$H = \frac{P_{\text{max}}}{A_c}, \quad (2)$$

$$E_r = \frac{S\sqrt{\pi}}{2\beta\sqrt{A_c}}, \quad (3)$$

where A_c is the corrected contact area, determined from prior calibration of the indenter tip in fused quartz, S is the stiffness at the initial unloading, P_{max} is the maximum load, and β is a constant which is related to the geometry of the indenter; the Berkovich tip has $\beta = 1.034$.

Nanoindentation was also used to examine the spatial distribution of residual stress in the specimen. Residual stress can lead to changes in pile-up around an indentation, leading to a perceived error in modulus due to pile-up area around the indentation not accounted for in the area calibration. By calculating a corrected contact area, the hardness and elastic modulus are independent of the residual stress.^{38,39} Residual stress additionally alters the load-depth curves. After cold working, materials exhibit a pile-up area around the indent point, which is the result of incompressibility after cold working.^{36,40,41} Based on the Suresh and Giannakopoulos

model,⁴¹ residual stress, σ_{SG} , in the sample can be found by comparing a stressed sample and a stress-free sample as the following equation:

$$\sigma_{\text{SG}} = H \left(\frac{A_0}{A} - 1 \right), \quad (4)$$

$$\sigma_{\text{SG}} = \frac{H}{\sin \alpha} \left(1 - \frac{A_0}{A} \right), \quad (5)$$

where Equation 4 represents a tensile residual stress and Equation 5 represents a compressive residual stress. For the same depth of indentation, the contact area, A , for the stressed sample with a tensile residual stress is smaller than the stress-free sample, A_0 , while bigger for compressive stress. There is a coefficient ($\sin \alpha$) in compressive residual stress equation, which is related to the effect of compressive residual stress on indentation tip, here for the Berkovich tip ($\alpha = 24.7^\circ$).⁴¹

3 | EFFECTS OF SHOT PEENING: SURFACE, SUBSURFACE DEPTH PROFILE, AND MICROSTRUCTURE

Figure 2A shows a plane view of the shot-peened surface via optical microscopy and indicates the dimpled pattern resulting from the media impacting the surface. Cracking is observed within the base of the impressions in Figure 2B. Figure 3A shows the surface topography measurement, while Figure 3B compares typical line traces of the baseline as machined sample face and a shot-peened sample face. The shot-peened surface has a peak to valley surface roughness of $\sim 10 \mu\text{m}$, whereas the baseline sample has a range of $\sim 2 \mu\text{m}$. In both Figures 2 and 3, the images and data correspond to the as shot-peened surface, prior to any mechanical polishing. Afterwards, as mentioned in Section 2.3, the shot-peened samples were polished to a depth of $\sim 90 \mu\text{m}$ to achieve a uniform, flat surface that is free of surface defects from the shot peening process.

The residual stress profile, extracted from nanoindentation profiles of the cross section of the material, is shown in Figure 4 and scaled to comply with the equilibrium condition (through thickness stress balance of tension and compression). Qualitatively the resultant residual stress profile is in agreement with the trend expected from literature. Overall, 78 nanoindents were obtained and each data point in Figure 4 represents the moving average of 6–8 nanoindent values over the thickness of the sample. X-ray diffraction was performed on both sides of the specimens, resulting in a compressive residual stress of $-194.6 \pm 13.7 \text{ MPa}$ and $-246.7 \pm 21.6 \text{ MPa}$ on each side, respectively. Based on the nanoindentation study, a compressive region of residual

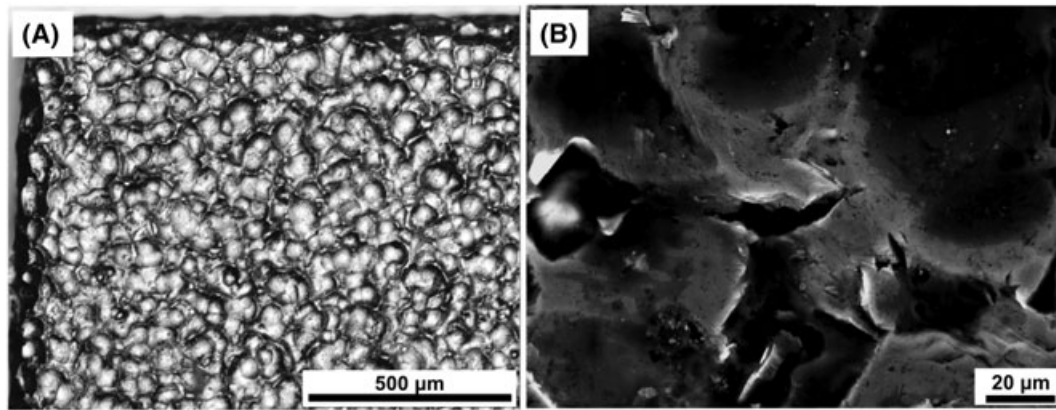


FIGURE 2 AA7050-T7541 sample of the as shot peened surface, prior to any polishing: A, optical microscopy view at 10 \times displaying well-defined indents due to shot peening and B, scanning electron microscope via at 800 \times , located at the base of an indent, displaying matrix cracking

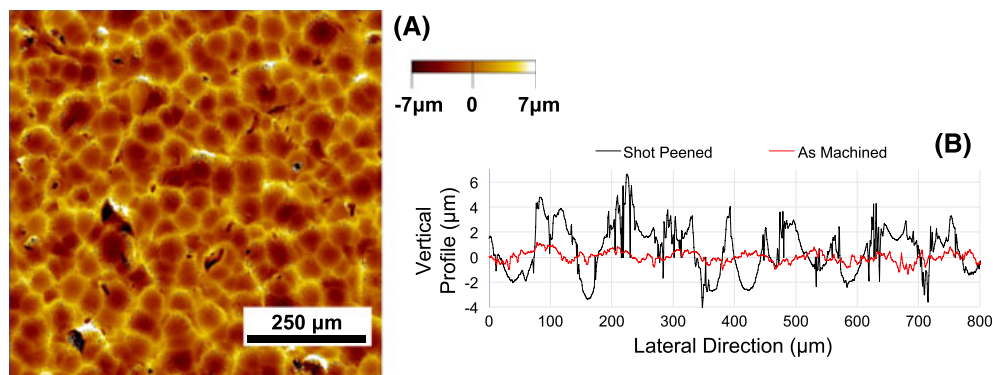


FIGURE 3 A, Top view topographic map of AA7050-T7541 following the shot peening process, prior to any polishing. B, Comparative surface topography line scan of the varied surface states in the shot peened and baseline conditions [Colour figure can be viewed at wileyonlinelibrary.com]

stress extends to a depth of approximately 200 and 400 μm from each surface, respectively. This asymmetric trend was noted within the XRD surface measurement results, however, in terms of near surface compressive stress magnitude, rather than depth of compressive residual stress penetration. This

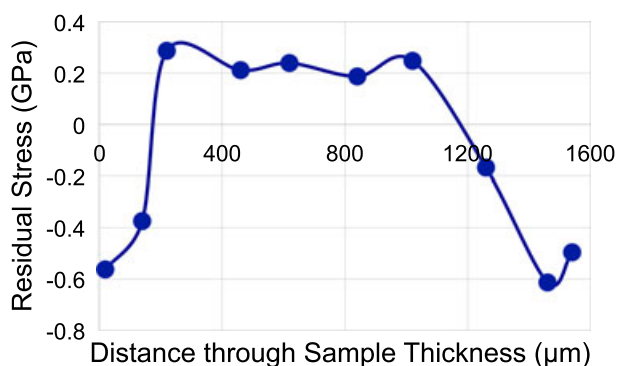


FIGURE 4 Through thickness (1.6 mm), qualitative residual stress profile of shot-peened AA7050-T7541 derived from nanoindentation force depth results using the Suresh and Giannakopoulos residual stress model³⁰ [Colour figure can be viewed at wileyonlinelibrary.com]

may be attributed to stress relaxation (through thickness wave propagation) during the staged peening process (peen flip peen). It is emphasized that the residual stress depicted in Figure 4 is intended to be a quick determination of the trends in the through thickness residual stress field of the sample using data obtained via nanoindentation and not a quantitative measurement of the residual stress values. Moreover, the Suresh and Giannakopoulos model for residual stress has been validated in the literature based on applied loading of thin films,³⁷ synchrotron-based XRD around scratches in Al,⁴² conventional lab-source XRD in steel⁴³ and metal matrix composites,⁴⁴ and Raman spectroscopy in thin carbon films.⁴⁵

To investigate the microstructure, a total of 4 EBSD scans were conducted on a 1 mm² area. Two scans were performed upon a baseline sample, and 2 scans were performed upon a shot-peened sample for the purposes of microstructural analysis and grain characterization. The inverse pole figure plots of the respective sample types can be seen in Figure 5A (baseline sample) and Figure 5B (shot-peened sample). Texture exists in the baseline sample (oriented in the L-T

direction) for the rolled material. It is evident that the microstructure exhibits significant grain elongation and texturing parallel to the L-T direction. The shot-peened sample exhibits a more random grain orientation, as the shot peening produces more grains with $\langle 001 \rangle$ orientations.

Grain size (diameter) between the pooled and cleaned shot-peened and baseline scans illustrate a relatively similar makeup (Figure 5D). A null hypothesis test was conducted to discern any significance in average grain size between the 2 sets and shows no statistical difference in average grain size for the analyzed areas of the baseline versus shot-peened samples. For each of the baseline and shot-peened sample scans, we observe an average grain diameter of 78.2 and 76.9 μm , respectively, when combining scan results of the same sample type. In literature, shot peening has been shown to have a profound effect upon grain structure, including grain refinement and severe plastic deformation.^{46,47} It is noted in Harada et al⁴⁶ and AlMangour et al⁴⁷ that the grain structure was analyzed at the shot-peened surface, while the grain refinement effect due to shot peening is not evident in the present results. This is attributed to the EBSD scans being taken after polishing to expose a peening subsurface of $\sim 90 \mu\text{m}$; as aforementioned²² and discussed in Section 4, the subsurface particle cracking is of primary interest in the present study.

4 | CRACKING OF $\text{Al}_7\text{Cu}_2\text{Fe}$ CONSTITUENT PARTICLES

Results of the energy dispersive X-ray spectroscopy elemental analysis showed that the precipitates are predominantly $\text{Al}_7\text{Cu}_2\text{Fe}$ in an Al matrix. Small inconsistent returns of magnesium (Mg) were also noted. To interrogate the evolution of

the constituent particles during fatigue loading in the baseline and shot-peened cases, SEM images of the particles were taken. As shown in Figure 6A and 6B, representative particles were imaged in the baseline samples prior to fatigue loading. The samples were polished to a uniform depth below the machining surface and vast majority of the particles were intact and display no visible damage. The baseline case was fatigue loaded and, after 5500 cycles, representative particles are shown in Figure 6C and 6D. Following the fatigue regime, the precipitates exhibit significant cracking, and incubation and propagation of said cracks into the material matrix is observed. The absence of any compressive residual stress field within the matrix results in propagation of the cracks extending into and throughout the Al matrix.

The shot-peened samples were polished to a depth of $\sim 90 \mu\text{m}$ beneath the shot peening surface, which is important relevant to subsurface precipitate cracking. Barter et al²² demonstrated that precipitates are the common sites for fatigue crack initiation, by surveying approximately a thousand fatigue cracks within baseline AA7050-T7451. The survey suggests that for a fatigue regime, that most of fatigue cracks initiating from precipitates that are located subsurface. With this in mind, we rationalize investigation of particle cracking in shot-peened specimens at a depth of $\sim 90 \mu\text{m}$ from the shot-peened surface. It should be noted that during the SEM image surveying, which all observed particles in the shot-peened condition, before fatigue loading, displayed evidence of cracking within the precipitate, as shown in Figure 7A and 7B. Following fatigue, the cracked precipitates are observed to be obliterated (Figure 7C and 7D), with significant cracking throughout. It is interesting to note that only minor debonding occurred with reference to the precipitate interaction with the matrix, without evidence of cracks extending into the material matrix itself, which is in stark

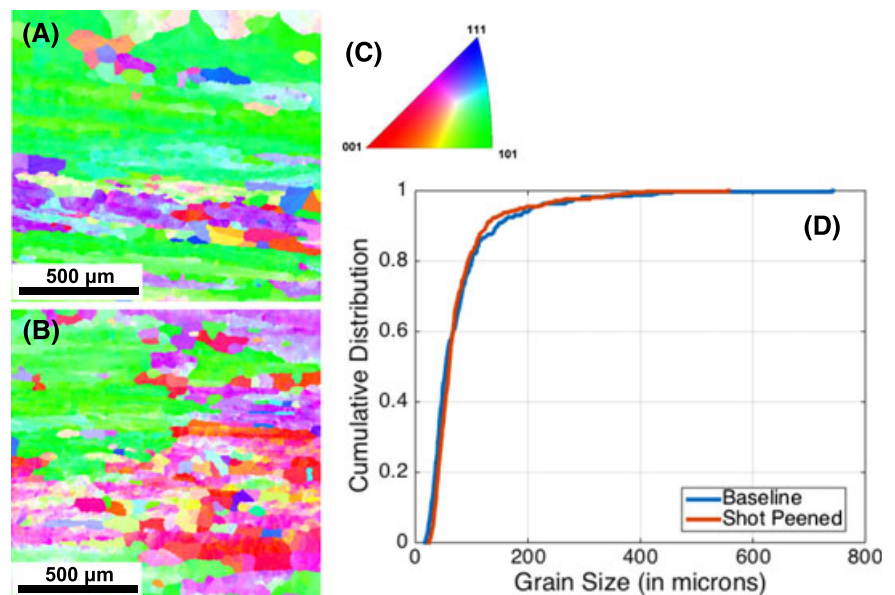


FIGURE 5 Shot-peened electron backscatter diffraction map of the A, baseline and B, shot peened samples; C, inverse pole figure color map; and D, cumulative distribution of grain diameters in both states [Colour figure can be viewed at wileyonlinelibrary.com]

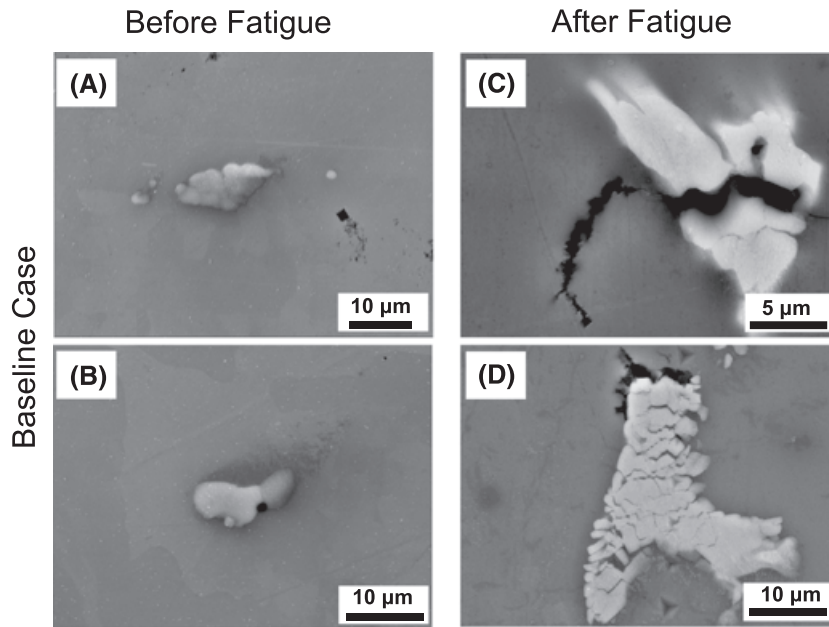


FIGURE 6 Scanning electron microscope image of AA7050-T7451 in the baseline condition. A and B, Intact precipitates before fatigue. C, A cracked precipitate demonstrating incubation and propagation into the material matrix following fatigue. D, An obliterated precipitate demonstrating debanding and crack propagation into the material matrix

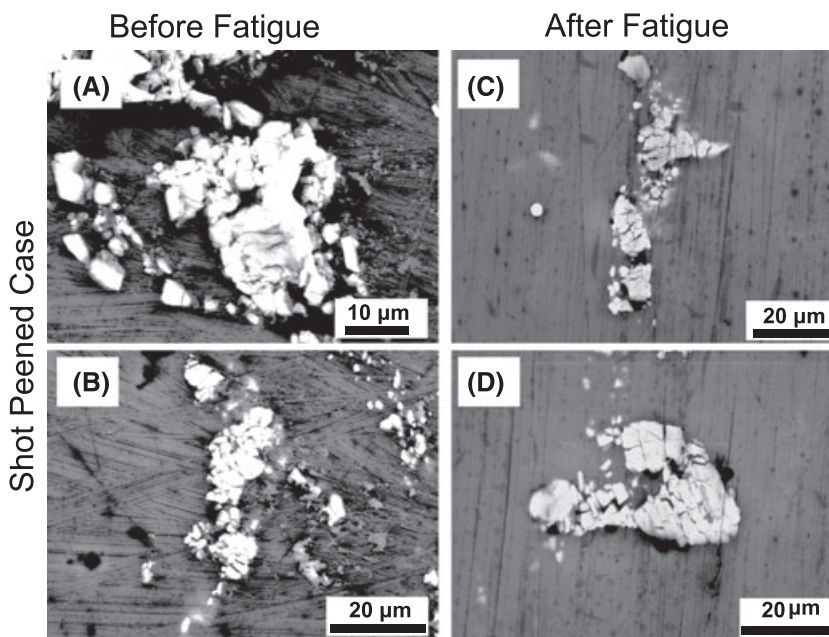


FIGURE 7 Scanning electron microscope image of AA7050-T7451 following the shot peening process, shown at $\sim 90\text{-}\mu\text{m}$ subsurface. A and B, Cracked precipitates before fatigue. C, A cracked precipitate following fatigue. D, a cracked precipitate following fatigue with evidence of debanding

contrast to the baseline case. It is theorized that the absence of these cracks extending into the matrix is due to the compressive residual stress field induced by shot peening, retarding the crack propagation into the material matrix; combined with the effect of cracked precipitates having a higher compliance due to the initially cracked state of all the shot-peened sample precipitates. This survey has provided qualitative evidence to suggest that while shot peening may initially crack precipitate particles in aerospace aluminum alloys, this detrimental effect is offset by the induced compressive residual stress induced by the process.

With this in mind, therein lies the potential to quantitatively analyze the competing effects of shot peening, inducing a compressive residual stress and cracking particles, throughout the fatigue life via nanoindentation. In each state, nanoindentation was conducted upon precipitates within the area of interest. Indentation pattern was in a straight line and each with a spacing of $10\ \mu\text{m}$, spanning enough interrogation points to traverse from one side of the precipitate within the material matrix, to the opposite side (usually involving 7-10 indents). It was attempted to place the central indents of the line, directly upon the precipitate center.

The precipitates were evaluated via quantification of the reduced modulus, according to Equation 3, from the indentation loading and unloading data. The nature of nanoindentation allows for the measurement of the reduced modulus at a very precise location, ideal for interrogating individual precipitates on the micrometer scale, indentations were made to depths no more than 300 nm, such that a residual impression of approximately 1 μm was made by any given indentation, therefore the modulus of the particles can be measured. For evaluation of the reduced modulus, E_r , only data points clearly within the boundary of the precipitate were selected as representative. Figure 8 illustrates the resultant reduced modulus distribution for the tested precipitate states, depicted as a cumulative distribution of the ensemble of test points for each case. Statistical variation is observed in the reduced modulus, which is typical of the nanoindentation measurement. The shot-peened reduced modulus is at the lower end of the spectrum, then followed by the baseline post fatigue state, and finally the baseline pre fatigue state. Since the Oliver and Pharr method assumes a uniform semi-infinite solid,³⁶ the presence of cracks can add compliance to the system, leading to a perceived modulus lower than that of the actual material. This order of modulus is qualitatively in agreement with the hypothesized cracking state, whereby, it is presumed that a higher extent of cracking within the precipitate particle, will result in a lower stiffness.

A key element of this research is to understand how a cracked particle starts to incubate the short crack into the matrix within a residual stress field. The critical difference in this research hypothesis is the existence of shot-peened cracked precipitates at the subsurface, prior to any fatigue cycling. The shot peening of the substrate causes elastic-plastic deformation and induces a compressive residual stress

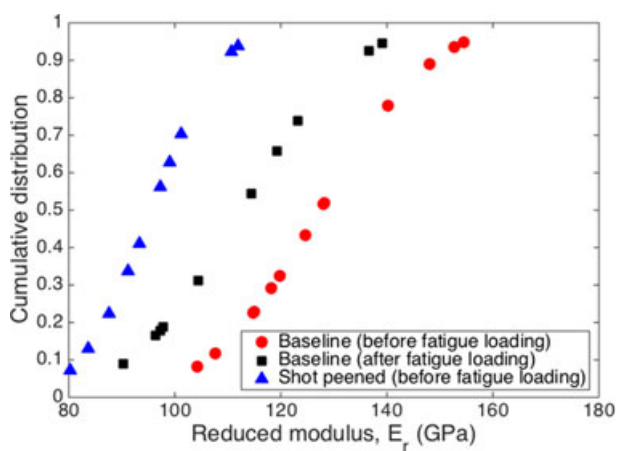


FIGURE 8 Cumulative distribution of the reduced modulus of the $\text{Al}_7\text{Cu}_2\text{Fe}$ precipitates measured by nanoindentation for the baseline samples (before and after fatigue) and the shot peened samples (before fatigue). Shot peening and fatigue loading act to crack the particles, resulting in a decrease in the particle's modulus [Colour figure can be viewed at wileyonlinelibrary.com]

field, however, detrimentally cracked hard constituent precipitate particles, as well as inducing surface damage. Limited literature exists to quantify the extent of this cracking; however, Bozek et al.²³ have conducted statistical analysis upon the cracking state of constituent particles (precipitates) of baseline AA7075-T651 following fatigue. A similar detailed study has not been carried out comparing the baseline state to that of shot peening, which is a contribution of the present paper.

5 | ROLE OF RESIDUAL STRESS IN THE AA7050 MATRIX

Residual stress measurements were conducted upon the front and rear faces of shot-peened samples, at the aforementioned seven stages of fatigue (at $N = 0, 1, 10, 100, 1000, 10\,000,$ and $15\,000$ cycles). As shown in Figure 9, this yielded a total of 14 results for the shot-peened samples; and for the baseline samples, 3 measurements were performed at varied stages of fatigue (at $N = 0, 100, 10\,000$ cycles). Following the fatiguing of samples and intermittent XRD residual stress measurements, we see some interesting results. Notably, there is a consistent differential in the compressive residual stress between the front and back face of the samples. This result may be attributable to the staged shot peening process, by which one face of the dog bone specimen is peened, then the specimen is turned for peening on the opposite side, resulting in an asymmetry due to the order of work hardening being done by the peening process, with the second peening step having a stress relaxation effect through the thickness of the thin specimen. Secondly, we note an asymmetric relaxation between the 2 surface faces of the compressive residual

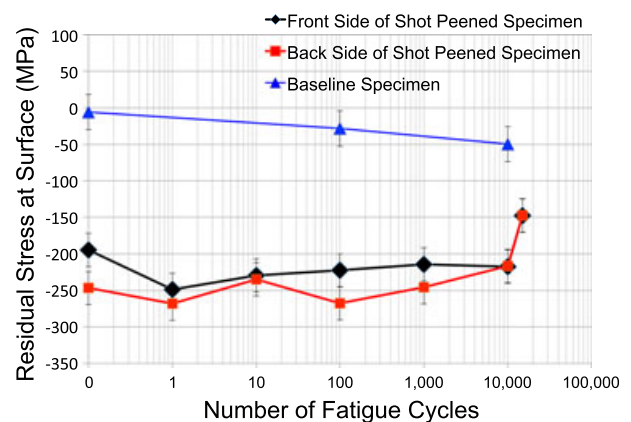


FIGURE 9 Evolution of the residual stress measurements during fatigue loading. Measurements are taken at the surface of the specimens via x-ray diffraction. Because of the staged shot peening process, a discrepancy is seen in residual stress from the front and back sides; in both cases, stress relaxation is observed prior to failure. The baseline case displays negligible residual stress [Colour figure can be viewed at wileyonlinelibrary.com]

stress magnitude through fatigue cycling for the shot-peened samples. Qualitatively, we see the higher absolute magnitude residual stress face relax earlier in fatigue than the lower absolute magnitude residual stress face. At the 10 000 cycle point, we also observe equilibrium of compressive residual stress between faces, and then a rapid symmetric relaxation through to the 15 000 cycle point. During cyclic loading, the residual stress field relaxes due to load shedding around microplasticity regions. Jhansale and Topper suggested a power law relationship for the residual stress relaxation rate with applied loading cycles, which their exponential material constant depends on the rate of cyclic hardening/softening and the applied load levels.⁴⁸ The residual stress relaxation has been analyzed and modeled for a range of shot-peened materials.^{8,9,49-52} Regarding the baseline result, we note a slight deviation through fatigue towards a compressive state. However, this is considered insignificant, and deemed to be within the realm of error. The baseline sample type remains in a relatively stress-free state throughout fatigue.

For a qualitative comparison, nanoindentation results depict the residual stress in the matrix of the material based on the Suresh and Giannakopoulos model.⁴¹ This model demonstrates that when a residual stress is present, the indentation load versus penetration depth curve translates compared to a stress-free virgin material. For this experiment, the baseline samples prior to fatigue were considered to be stress free (as appropriately determined based on the XRD results in Figure 9). The stress-free condition (baseline sample before fatigue loading) was considered as the average of many measurements taken in the matrix adjacent to the precipitates (as this is the key area of interest leading to incubation of a propagating crack). In representing the qualitative residual stress of the material matrix for the states of the samples, the indentation load versus indent penetration depth must be graphically demonstrated (Figure 10). The

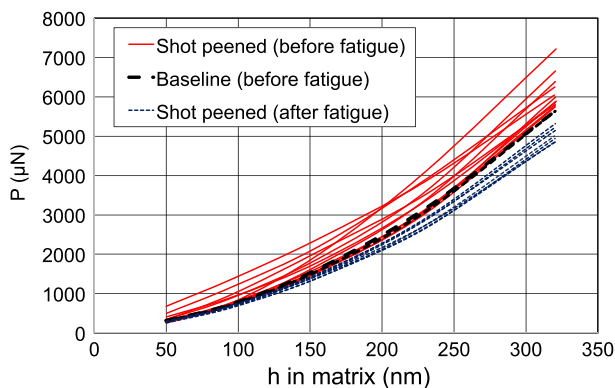


FIGURE 10 The indentation load versus penetration depth curve for shot peened samples, compared with a presumed stress free baseline material (average of many baseline measurements), illustrating the compressive residual stress before fatigue and relaxation after fatigue loading [Colour figure can be viewed at [wileyonlinelibrary.com](#)]

shot-peened sample prior to fatigue loading illustrates the translation upward and to the left in the indentation load versus penetration depth curve for a compressive residual stress, compared to the stress free virgin material. We note that for a tensile residual stress, a shift downward and to the right on the plot is observed, as is the case for the shot-peened sample after fatigue loading. In the representation of residual stress for the material matrix, only indents clearly within the matrix were used as data points. Figure 10 illustrates the material matrix qualitative residual stress measurement resulting from nanoindentation; hence, a compressive residual stress bias for the shot-peened sample, prior to fatigue, is exhibited, as expected based on theory and correlation with the XRD results. Additionally, we see a relaxation through fatigue, with the shot-peened sample curves in an orientation closer to the stress-free state than the compressive residual stress observed in the pre-fatigue case.

Within the matrix of the baseline samples in the vicinity of the precipitates, the reduced modulus, E_r , is measured via nanoindentation, according to Equation 3. Figure 11 represents cumulative distribution of the reduced modulus values in the matrix before and after fatigue. During the cyclic loading, a significant drop in the reduced modulus of the matrix is observed. As shown in Figure 6C and 6D after fatigue, cracks were seen to incubate from the precipitate into the matrix. The reduced modulus was measured adjacent to the propagating crack (Figure 11) and as expected resulted in a further reduction in the values of E_r , which represents the higher compliance exhibited by the material due to the introduction of the free surface of the crack. For quantitative comparison, the shot-peened sample after fatigue has

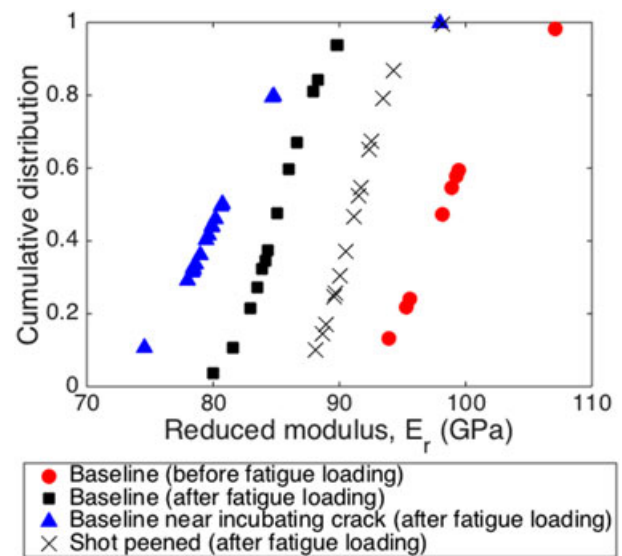


FIGURE 11 Cumulative distribution of the reduced modulus of the matrix measured by nanoindentation for the baseline (before and after fatigue) and shot peened (after fatigue) samples in the vicinity of particles, as well as near an incubating crack after fatigue [Colour figure can be viewed at [wileyonlinelibrary.com](#)]

considerably higher reduced modulus than its baseline counterpart. The compressive residual stress field induced by shot peening represents the rationale for the higher values of E_r , and the resistance from a crack particle to incubate and grow this crack into the matrix of the shot-peened sample.

6 | CONCLUSIONS

This work has provided the foundation for crack initiation and crack incubation by precipitates within shot-peened aluminum alloys, specifically AA7050-T7451. Surface topography following shot peening quantified the resulting surface roughness. Grain characterization noted no discernable difference in microstructure between shot-peened and baseline samples, in terms of grain size at a subpeening depth of $\sim 90\ \mu\text{m}$. Elemental analysis has demonstrated the chemical constituents of precipitate particles within AA7050-T7451 are predominantly comprised of $\text{Al}_7\text{Cu}_2\text{Fe}$.

Damage tolerant analysis is used to determine the fatigue life in aerospace components, which relies on the description of an initial defect size. A significant outcome of this work is the quantification of the initiation and incubation of cracks within the particles in the baseline sample versus the inability to incubate cracks from cracked particles in the shot-peened sample. The effect of shot peening upon the state of damage in the precipitates demonstrated that subsurface particle cracking (at $\sim 90\ \mu\text{m}$ from the shot-peened surface) is evident via surface preparation and SEM imaging of precipitates in shot-peened samples. Near surface residual stresses have been evaluated through XRD measurement in shot-peened samples, as a function of the fatigue evolution, demonstrating rapid relaxation of near surface residual stresses leading to the reduction in beneficial (crack retarding) compressive residual stress. Further, sequential shot peening for each side of the thin specimen (1.6 mm) resulted in surface residual stresses of $-194.6 \pm 13.7\ \text{MPa}$ and $-246.7 \pm 21.6\ \text{MPa}$ on the front and back, respectively, from XRD measurements and subsurface compression depths of approximately 200 and 400 μm from each surface, as characterized by nanoindentation.

The SEM survey of precipitates confirmed the cracked state of precipitates in the shot-peened samples, prior to fatigue loading, demonstrating the adverse effect of shot peening damage. This cracked state has been quantified utilizing nanoindentation techniques, specifically the perceived reduced modulus in the precipitates and matrix for the baseline and shot-peened cases, before and after fatigue. As expected the reduced modulus quantified the consequence of cracking the precipitates in the shot-peened sample prior to fatigue loading; the overall stiffness of the intermetallic particles decreases by 25% after shot peening due to particle fracture. But incubation and growth of cracks into the matrix

after fatigue is easier in the baseline sample than the shot-peened sample, as the baseline matrix is 7% more compliant than the shot-peened matrix.

ACKNOWLEDGEMENTS

DJC acknowledges support from this work under a MS thesis program between the Royal Australian Air Force and Purdue University. All authors gratefully acknowledge support provided by Purdue's Center for Surface Engineering and Enhancement. MDS acknowledges funding from the Office of Naval Research, N00014-14-1-0544. The authors would like to thank Mr. Jack Champagne (Electronics Incorporated) and Mr. Jim Whalen (Progressive Surface) for conducting the shot peening; Dr. Alberto Mello and John Rotella for their help with microstructure characterization, surface roughness assessment, and fatigue testing; Raheleh M. Rahimi for conducting the nanoindentation; and Dr. Mauro Sardela for help with X-ray diffraction (performed at the Frederick Seitz Materials Research Laboratory Central Research Facilities, University of Illinois).

REFERENCES

1. Elber W. The effects of shot peening residual stresses on the fracture and crack growth properties of D6AC steel. NASA Langley Research Centre, Report No. TM X-71943. 1974.
2. Curtis S, De los Rios ER, Rodopoulos CA, Levers A. Analysis of the effect of controlled shot peening on fatigue damage of high strength aluminum alloys. *Int J of Fatigue*. 2003;25:59.
3. Rodopoulos CA, Curtis SA, de los Rios ER, SolisRomero J. Optimisation of the fatigue resistance of 2024-T351 aluminum alloys by controlled shot peening—methodology, results, and analysis. *Int J Fatigue*. 2004;26:849.
4. Benedetti M, Bortolamedi T, Fontanari V, Frendo F. Bending fatigue behavior of differently shot peened Al 6082 T5 alloy. *Int J Fatigue*. 2004;26:889.
5. Torres MAS, Voorwald HJC. An evaluation of shot peening, residual stress, and stress relaxation on the fatigue life of AISI 4340 steel. *Int J Fatigue*. 2002;24:877.
6. Everett RA, Matthews WT, Prabhakaran R, Newman JC, Dubberly MJ. The effects of shot and laser peening on crack growth and fatigue life in 2024 aluminum alloy and 4340 steel. NASA Report. 2001.
7. Sharp PK, Clark G. *The Effect of Peening on the Fatigue Life of 7050 Aluminum Alloy*. Aeronautical and Maritime Research Laboratory, Australian Government; 2001.
8. Meguid SA, Shagal G, Stranart JC, Liew KM, Ong LS. Relaxation of peening residual stresses due to cyclic thermo-mechanical overload. *J Eng Mater Technol, Trans ASME*. 2005;127(2): 170-178.
9. Yanhuai L, Jian L, Kewei X. Calculation of relaxation of residual stress and change of yield strength in shot peened layer. *Mater Sci Forum*. 2005;490-491:396-403.

10. Gao Y-k, Li X-b, Yang Q-x, Yao M. Influence of surface integrity on fatigue strength of 40CrNi2Si2MoVA steel. *Mater Lett.* 2007; 61(2):466-469.
11. Oguri K. Fatigue life enhancement of aluminum alloy for aircraft by fine particle shot peening (FPSP). *J Mater Process Technol.* 2011;211:1395-1399.
12. Book TA, Sangid MD. Evaluation of select surface processing techniques for in situ application during the additive manufacturing build process. *JOM.* 2016;68:1780-1792.
13. Matsui K, Eto H, Yukitake K. Increase in fatigue limit of gears by compound surface refining using vacuum carburizing, contour induction hardening and double shot peening. *JSME Int J Series A-Solid Mech and Mat Eng.* 2002;45:290-297.
14. Luong H, Hill MR. The effects of laser peening and shot peening on high cycle fatigue in 7050-T7451 aluminum alloy. *Mat Sci and Eng.* 2010;527:699-707.
15. O'Hara P. Superfinishing and shot peening of surfaces to optimise roughness and stress. *WIT Transactions on Engng Sci.* 1970;25: 321-330.
16. Sangid MD, Stori JA, Ferreira PM. Process characterization of vibrostrengthening and application to fatigue enhancement of aluminum aerospace components—part I. Experimental study of process parameters. *Int J of Adv Manufacturing Tech.* 2011;53.5-8:545-560.
17. Sangid MD, Stori JA, Ferreira PM. Process characterization of vibrostrengthening and application to fatigue enhancement of aluminum aerospace components—part II: Process visualization and modeling. *Int J of Adv Manufacturing Tech.* 2011;53.5-8:561-575.
18. Xiang Y, Liu Y. Mechanism modelling of shot peening effect on fatigue life prediction. *Fat Fract Engin Mater Struct.* 2010;33: 116-125.
19. Bagherifard S, Ghelichi R, Guagliano M. Numerical and experimental analysis of surface roughness generated by shot peening. *Appl Surf Sci.* 2012;258:6831-6840.
20. Mylonas GI, Labeas G. Numerical modelling of shot peening process and corresponding products: residual stress, surface roughness and cold work prediction. *Surf Coatings Technol.* 2011;205:4480-4494.
21. Akyildiz HK, Kulekci MK, Esme U. Influence of shot peening parameters on high-cycle fatigue strength of steel produced by powder metallurgy process. *Fat Fract Engin Mater Struct.* 2015;38:1246-1254.
22. Barter SA, Sharp PK, Holden G, Clark G. Initiation and early growth of fatigue cracks in an aerospace aluminium alloy. *Fatigue Fract Engng Mater Struct.* 2002;25:111-125.
23. Bozek JE, Hochhalter JD, Veilleux MG, et al. A geometric approach to modeling microstructurally small fatigue crack formation: I. Probabilistic simulation of constituent particle cracking in AA 7075-T651. *Modelling and Simulation in Mat Sci and Engng.* 2008;16(6):065007.
24. Hochhalter JD, Littlewood DJ, Christ RJ Jr, et al. A geometric approach to modeling microstructurally small fatigue crack formation: II. Physically based modeling of microstructure-dependent slip localization and actuation of the crack nucleation mechanism in AA 7075-T651. *Modelling and Simulation. in Mat. Sci. and Engng.* 2010;18(4):045004.
25. Hochhalter JD, Littlewood DJ, Veilleux MG, et al. A geometric approach to modeling microstructurally small fatigue crack formation: III. Development of a semi-empirical model for nucleation. *Modelling and Simulation in Mat Sci and Engng.* 2011;19(3): 035008.
26. Prasannavenkatesan R, Zhang J, McDowell DL, Olson GB, Jou HJ. 3D modeling of subsurface fatigue crack nucleation potency of primary inclusions in heat treated and shot peened martensitic gear steels. *Int J Fatigue.* 2009;31(7):1176-1189.
27. Zhang J, Prasannavenkatesan R, Shenoy MM, McDowell DL. Modeling fatigue crack nucleation at primary inclusions in carburized and shot-peened martensitic steel. *Engng Fract Mechanics.* 2009;76(3):315-334.
28. Luong H, Hill MR. The effects of laser peening and shot peening on high cycle fatigue in 7050-T7451 aluminum alloy. *Mater Sci and Eng: A.* 2010;527:699-707.
29. Carvalho ALM, Voorwald HJC. Influence of shot peening and hard chromium electroplating on the fatigue strength of 7050-T7451 aluminum alloy. *Int J Fat.* 2007;29:1282-1291.
30. Carvalho ALM, Voorwald HJC. The surface treatment influence on the fatigue crack propagation of Al 7050-T7451 alloy. *Mater Sci Eng A.* 2009;505:31-40.
31. Gao YK. Improvement of fatigue property in 7050-T7451 aluminum alloy by laser peening and shot peening. *Mater Sci and Eng: A.* 2011;528:3823-3828.
32. Bae H. Experimental study of shot peening process and its effects on high cycle fatigue in aero space materials. PhD Thesis: University of Washington. 2011.
33. Society of Automotive Engineers. *Aerospace Material Specification – AMS 4050 Aluminum Alloy Plate (7050-T7451).* Society of Automotive Engineers; 1974.
34. ASTM E8/E8M-13a. Standard test methods for tension testing of metallic materials. *ASTM International.* 2013;01-28.
35. Mello AW, Nicolas A, Lebensohn RA, Sangid MD. Effect of microstructure on strain localization in a 7050 aluminum alloy: comparison of experiments and modeling for various textures. *Mat Sci and Engng.* 2016;661:187-197.
36. Oliver WC, Pharr GM. An improved technique for determining hardness and elastic modulus using load and displacement sensing indentation experiments. *J Mater Res.* 1992;7:1564.
37. Oliver WC, Pharr GM. Measurement of hardness and elastic modulus by instrumented indentation. Advances in understanding and refinements to methodology. *J Mater Res.* 2004;19:3.
38. Hay JC, Bolshakov A, Pharr GM. A critical examination of the fundamental relations used in the analysis of nanoindentation data. *J Mater Res.* 1999;14:2296.
39. Cheng YT, Cheng CM. Can stress-strain relationships be obtained from indentation curves using conical and pyramidal indenters. *Int J Solids Structures.* 1999;36:1231
40. Nishikawa M, Soyama H. Two-step method to evaluate equibiaxial residual stress of metal surface based on microindentation tests. *Mater Des.* 2011;32:3240.
41. Suresh S, Giannakopoulos AE. A new method for estimating residual stresses by instrumented sharp indentation. *Acta Mater.* 1998;46:5755-5767.

42. Khan MK, Fitzpatrick ME, Hainsworth SV, Evans AD, Edwards L. Application of synchrotron X-ray diffraction and nanoindentation for the determination of residual stress fields around scratches. *Acta Mater*. 2011;59:7508-7520.
43. Zhu L-N, Xu B-S, Wang H-D, Wang C-B. Measurement of residual stress in quenched 1045 steel by the nanoindentation method. *Mater Char*. 2010;61:1359-1362.
44. Jeong SG, Park JH, Jang JH, Han KS. Measurement of residual stress in A356/SiCP metal matrix composite by nanoindentation. 18th Int. Conf. of Comp. Mat. 2005:1-4.
45. Taylor CA, Wayne MF, Chiu WKS. Residual stress measurement in thin carbon films by Raman spectroscopy and nanoindentation. *Thin Solid Films*. 2003;429:190-200.
46. Harada Y, Fukaura K, Tsuchida N. Grain refinement of metal surface using hot shot peening, *Materials Science Forum ISSN: 1622-9752 Vols. 539-543, Trans Tech Publications*. 2007: 1080-1085.
47. AlMangour B, Yang. Improving the surface quality and mechanical properties by shot-peening of 17-4 stainless steel fabricated by additive manufacturing. *Materials & Design*. 2016;110: 914-924.
48. Jhansale HR, Topper TH. Engineering analysis of the inelastic stress response of a structural metal under variable cyclic strains, cyclic stress-strain behavior—analysis, experimentation, and failure prediction. *Amer Soc Test Mat*. 1973;2:111-118.
49. Foss BJ, Gray S, Hardy MC, Stekovic S, McPhail DS, Shallock BA. Analysis of shot-peening and residual stress relaxation in the nickel-based superalloy RR1000. *Acta Mater*. 2013;61:2548-2559.
50. Benedetti M, Fontanari V, Scardi P, Ricardo CLA, Bandini M. Reverse bending fatigue of shot peened 7075-T651 aluminium alloy: the role of residual stress relaxation. *Int J Fat*. 2009;31:1225-1236.
51. McClung RC. A literature survey on the stability and significance of residual stresses during fatigue. *Fatigue Fract Eng Mater Struct*. 2007;30:173-205.
52. You C, Achintha M, Soady KA, Smyth N, Fitzpatrick ME, Reed PAS. Low cycle fatigue life prediction in shot-peened components of different geometries—part I: residual stress relaxation. *Fatigue Fract Eng Mater Struct*. 2016;00:1-15.

How to cite this article: Chadwick DJ, Ghanbari S, Bahr DF, Sangid MD. Crack incubation in shot peened AA7050 and mechanism for fatigue enhancement. *Fatigue Fract Eng Mater Struct*. 2017. <https://doi.org/10.1111/ffe.12652>